Age-Specific 18F-FDG Image Processing Pipelines and Analysis Are Essential for Individual Mapping of Seizure Foci in Paediatric Patients with Intractable Epilepsy

Bianca De Blasi[1], Anna Barnes[2], Ilaria Boscolo Galazzo[3], Chia-ho Hua[4], Barry Shulkin[5], Matthias Koepp[6], Martin Tisdall[7]

[1]Dept. of Medical Physics, UCL, London, [2]Institute of Nuclear Medicine UCLH, London, [3]Dept. of Computer Science, University of Verona, Verona, [4]Dept. of Radiation Oncology, St. Jude Children's Research Hospital, Memphis, [5]Dept. of Diagnostic Imaging, St. Jude Children's Research Hospital, Memphis, [6]UCL Institute of Neurology, London, [7]Great Ormond Street Hospital, London

Bianca De Blasi, 33 Queen Square WC1N3BG London, UK, +447873543295, bianca.blasi.15@ucl.ac.uk, PhD student

Word count: 5000

Age-specific Analysis of Paediatric PET

ABSTRACT

Fluoro-18-deoxyglucose positron emission tomography (FDG-PET) is an important tool for the pre-surgical assessment of children with drug-resistant epilepsy. Standard assessment is carried out visually and this is often subjective and highly user-dependent. Voxel-wise statistics can be used to remove user-dependent biases by automatically identifying areas of significant hypo/hyper-metabolism, associated to the epileptogenic area. In the clinical settings, this analysis is carried out using commercially available software. These software packages suffer from two main limitations when applied to paediatric PET data: 1) paediatric scans are spatially normalised to an adult standard template and 2) statistical comparisons use an adult control dataset. The aim of this work is to provide a reliable observer-independent pipeline for the analysis of paediatric FDG-PET scans, as part of pre-surgical planning in epilepsy.

Methods. A pseudo-control dataset (n=19 for 6-9y, n=93 for 10-20y) was used to create two age-specific FDG-PET paediatric templates in standard paediatric space. The FDG-PET scans of 46 epilepsy patients (n=16 for 6-9y, n=30 for 10-17y) were retrospectively collated and analysed using voxel-wise statistics. This was implemented with the standard pipeline available in the commercial software Scenium and an in-house Statistical Parametric Mapping v.8 (SPM8) pipeline (including age-specific paediatric templates and normal database). A kappa test was used to assess the level of agreement between findings of voxel-wise analyses and the clinical diagnosis of each patient. The SPM8 pipeline was further validated using post-surgical seizure-free patients.

Results. Improved agreement with the clinical diagnosis was reported using SPM8, in terms of focus localisation, especially for the younger patient group: kScenium=0.489 versus kSPM=0.805. The proposed pipeline also showed a sensitivity of ~70% in both age ranges, for the localisation of hypo-metabolic areas on paediatric FDG-PET scans in post-surgical seizure-free patients.

Conclusions. We show that by creating age-specific templates and using paediatric control databases, our pipeline provides an accurate and sensitive semi-quantitative method for assessing FDG-PET scans of patients under 18y.

Keywords: Paediatric FDG-PET template, Voxel-wise statistics, Epilepsy

INTRODUCTION

Multi-modal imaging in patients with drug-resistant epilepsy is used to guide pre-surgical assessment in potential candidates for surgery *(1)*. This is a challenging procedure which aims to precisely localise the epileptogenic focus and its relation to the surrounding cortex and thus direct subsequent surgical resection. Despite fluoro-18-deoxyglucose positron emission tomography computed tomography (FDG-PETCT) being used since the 1980s to detect hypo-metabolism associated to the epileptogenic zone *(2,3)*, there are several methodological constraints, which limit its use, particularly in the paediatric population.

FDG-PET data are routinely assessed visually by expert readers. This qualitative evaluation is subjective and highly user-dependent, it might miss subtle or bilateral intensity changes and its effectiveness varies with epilepsy type and focus location *(2)*. More sophisticated voxel-wise statistical methods can be used to remove user-dependent biases, thereby improving reproducibility and preventing disagreement arising from visual assessment of PET scans *(2)*. These methods perform spatial normalization of the patient brain scan to a common standard template where it is compared to a normative dataset. This voxel-wise comparison leads to the automatic identification of areas of hypo/hyper-metabolism at the individual level. In adults (above 18 y) voxel-wise statistics has proven robust and reliable *(4–6)*. In paediatric patients, the efficacy of this analysis remains less clear due to age-related variation in brain size and metabolism. Only few studies have used age-matched paediatric databases for statistical comparison while detailed description of a paediatric FDG-PET template for spatial normalization is still missing *(2,7)*.

Voxel-wise analysis is usually carried out using FDA-approved automated software packages provided by Siemens (Scenium) or GE Healthcare (CortexID). Despite being user-friendly and highly intuitive, these software applications suffer from two main limitations when

applied to paediatric PET data: 1) the spatial normalization of the paediatric scans to adult Montreal Neurological Institute (MNI) standard space *(8)*, which leads to unwanted deformations and marked anatomical mismatches between the different brain structures and 2) the use of an adult in-built normative database for statistical comparisons which differs from children in both brain size and metabolism.

In this study, we investigated whether more accurate and reliable results can be achieved using age-specific templates and databases of FDG-PET images and we introduced a processing pipeline which aims at improving the accuracy of localising the epileptogenic zone on paediatric FDG-PET scans. Our aim was to create FDG-PET templates representing two age ranges (6-9 y and 10-20 y) and use age-appropriate control datasets for voxel-wise analysis. This pipeline was quantitatively compared against the commercial software Scenium, currently adopted in clinical settings and further validated using post-surgical seizure-free patients whose clinical follow-up diagnosis was used as gold standard.

METHODS

The adopted methodology included the voxel-wise analysis of a paediatric patient dataset, using a commercial software and an ad-hoc pipeline based on the Statistical Parametric Mapping v.8 (SPM8, http://www.fil.ion.ucl.ac.uk/spm/) pipeline. For the latter, we built two age-specific FDG-PET templates in the paediatric standard space defined by magnetic resonance imaging (MRI) templates, available from the paediatric atlas *(9)*. In the SPM8 pipeline, the patients' scans were compared to an age-matched pseudo-control database (i.e. without central nervous system diseases).

Study Population

The patient dataset was retrospectively collated from Great Ormond Street Hospital and includes FDG-PETCT scans of 46 children (n=16, 6-9 y and n=30, 10-17 y) with focal and generalised epilepsies, which reflects what is normally found in pre-surgical assessments (Supplemental Table 1 for patients' demographics). Of these patients, 18 (n=4, 6-9 y and n=14, 10-17 y) underwent surgical resection of the hypothesised epileptogenic area, with known surgical outcome reported on average 11 months after surgery (range of follow-up reports: 1-38 months). Pre-operative MRI scans were collected for all these patients while post-surgery scans (at least 6 months follow-up) were available in 13 cases (n=4, 6-9 y and n=9, 10-17 y).

Fig. 1 summarises the dataset under investigation and the corresponding analyses carried out. A control dataset (n=112, 6-20 y) was also included in the study, previously described in *(10)*. The research and development board at Great Ormond Street Hospital approved this retrospective study and the requirement to obtain informed consent was waived.

FDG-PET Acquisition

The patient dataset includes dedicated FDG-PETCT brain scans performed on subjects who fast 4 hrs before scanning. 18F-FDG was administered based on patient's weight (dose range: 14-200 Mbq), 30 min before scanning. FDG-PETCT images were acquired for 15 min using a Discovery 710 system (GE Healthcare). Attenuation-corrected PET images were iteratively reconstructed by standard vendor-provided software, using a voxel size of 2x2x3.27 mm^3.

The control dataset comprises whole body FDG-PETCT scans of patients referred for oncology staging, but displaying no brain pathology (pseudo-controls) *(10)*. We only considered the brain sections of these scans. FDG-PETCT scanning of this data was performed using a Discovery 690 PETCT system (GE Healthcare) at multiple bed positions in 3D mode for 3-5 min bed position *(10)*. Attenuation-corrected PET images were iteratively reconstructed by standard vendor-provided software, using a voxel size of 3.65x3.65x3.27 mm^3. For the complete description of the acquisition protocol and parameters please refer to *(10)*.

Creation of Paediatric Templates

The first objective of this study was to create age-specific paediatric FDG-PET templates in standard paediatric space and use them as reference for spatially normalising each scan before statistical analysis. Two asymmetric T1-weighted MRI standard templates of children between the age of 7-11 y (derived from n=112) and 13-18.5 y (derived from n=108) were used, from the paediatric atlas *(9)*. These structural templates defined the standard paediatric space on which to build the corresponding age-matched FDG-PET templates. The FDG-PET pseudo-control dataset was divided into two groups: children of age 6-9 y (n=19) and 10-20 y (n=93). The cut-off point of 10 years old was chosen based on the assumption that at this age brain glucose metabolism of children starts decreasing towards adult levels *(2)*. The following steps were carried in FSL

(https://fsl.fmrib.ox.ac.uk/fsl/fslwiki/), for the two age groups separately. The control scans were registered to the corresponding T1 MRI template (affine registration, 12 degrees of freedom) with mutual information as cost function (Registration1) *(11)*. The resulting registrations were visually assessed, using several anatomical landmarks as reference. Successful registrations were those where the PET was completely and precisely overlaid on the T1 image, especially over the frontal and temporal lobes. Then, an average of the correctly registered PET scans (Average1) was computed. A second registration was carried out to register all the control PET scans to Average1 (affine registration, 12 degrees of freedom) with correlation ratio as cost function (Registration2). The goodness of fit of Registration2 was again visually assessed for each control scan. An average of the correctly registered PET scans (Average2) was finally computed. The resulting two PET templates (one per age range) were considered for the spatial normalization of all the corresponding age-matched scans before voxel-wise statistics.

Voxel-Wise Statistical Analysis

Voxel-wise analysis produces statistical parametric maps highlighting regions on a patient's scan with significantly different metabolism compared to controls *(2)*. This was carried out using Scenium, a FDA approved, fully automated software currently available in clinical settings (Syngo.Via.v11 platform, Siemens) and predominantly used for the pre-surgical evaluation of epilepsy patients by comparing them with an in-built adult control dataset (FDG Biograph, 19-44 y) *(12)*. Single subject voxel-wise analysis was also carried out using a customized pipeline based on SPM8, an open source suite of MATLAB based routines where our in-house paediatric FDG-PET templates and control database could be easily integrated. The two pipelines and related processing steps are reported in **Fig. 2**.

Overall, both pipelines included smoothing of the patients' scans (12-mm fixed kernel in Scenium and 6-mm kernel in SPM8) spatial normalization to standard space (in-built adult MNI 91x109x91, 2-mm isotropic in Scenium and paediatric MNI 197x233x189, 1-mm isotropic in SPM8) and subsequent intensity normalization (by the mean global uptake in Scenium with limited possibility of change and by the cerebellum grey matter uptake *(3)* in SPM8). A single subject against control group two-sample t-test was carried out. In Scenium, this led to statistical maps which were displayed as colour maps, stereotactic projections or coronal views. An actual quantification of these results was given by statistics tables showing the number of standard deviations (SDs) away from the mean (control uptake) for a standard list of brain regions (Harvard Brain Atlas, keeping the right and left hemispheres separate, 10 regions each). We took as significant, those areas displaying the number of SDs less than -2 (95% confidence interval), i.e. reduced glucose metabolism than controls. In SPM8, the statistical maps were displayed using a p-value<0.001 (uncorrected) and a cluster extent k=100.

Comparison with Clinical Diagnosis

The agreement between the results from the voxel-wise analyses (Scenium/SPM8) and the clinical diagnosis was assessed by a neurosurgeon, with ten years of experience in paediatric epilepsy. This procedure was carried out by comparing the results of Scenium/SPM8 with the corresponding clinical diagnosis from the multi-disciplinary team (MDT), established on the basis of clinical information, electrophysiological and imaging findings. In the case of focal epilepsies, the area considered was the one with the highest negative Z-score (Scenium) and the one showing the lowest peak-level p-value (SPM8). We considered generalised those cases when more than three regions in different lobes were detected as significant on either of the statistical maps. A Kappa test was carried out to assess the level of agreement between each pipeline and the MDT

diagnosis when focus lateralisation (right, left, normal, multifocal) or localisation (frontal, temporal, parietal/occipital, normal, multifocal) were considered. Slight agreement is defined for kappa values between 0.01-0.20, fair agreement for 0.21-0.40, moderate agreement for 0.41-0.60, substantial agreement for 0.61-0.80 and almost perfect agreement for values 0.81-0.99 *(13)*.

Validation Using Post-Surgical Patients

In order to further validate the ad-hoc pipeline based on SPM8, we considered a subgroup of 18 subjects (n=4, 6-9 y and n=14, 10-17 y) who underwent surgical resection of the hypothesised focus and had known outcome. This was defined following Engel classification where seizure-free outcome corresponds to class I and non seizure-free to class II to IV. Patients who were seizure-free after surgery (n=3, 6-9 y and n=10, 10-17 y) were considered as gold standard (localisation of the epileptogenic area could be accurately ascertained) and included in the following analysis. Post-surgery scans were available in 10 cases (n=3, 6-9 y and n=7, 10-17 y, **Fig. 1**).

Each subject was analysed using the aforementioned SPM8 pipeline and the resulting statistical maps were co-registered to the corresponding pre-surgical MRI scan, together with the FDG-PET and post-surgical MRI scan. Then, the correct lateralisation and localisation of the statistical maps to the resection cavity was assessed. Correct lateralisation (localisation) was considered when the cluster containing the maximum on the statistical map fell in the hemisphere ipsilateral to the resected area (in the resected area). Sensitivity was separately defined for lateralisation and localisation as the proportion of cases where the maximum correctly lateralised or co-localised with the resected area. In the cases where post-surgical MRI scans were not available (n=3, 10-17 y), the statistical maps were co-registered to the pre-surgical MRI scan and lateralisation/localisation was visually assessed by the same neurosurgeon using surgery reports.

To provide a further quantification of the degree of overlap, the percentage of voxels in the most significant cluster which were falling within the resected area was calculated (**Fig. 1**). The lesion was segmented out from the post-surgical MRI scan of each subject, using ALI toolbox (http://www.fil.ion.ucl.ac.uk/spm/ext/#ALI) customised with paediatric templates and tissue priors. This lesion segmentation was used to mask the statistical map in order to calculate the proportion of voxels falling in the resected area.

In the five non seizure-free patients (n=1, 6-9 y and n=4, 10-17 y), our findings were visually compared to the area resected to evaluate the FDG-PET in these cases (**Fig. 1**).

RESULTS

Creation of Paediatric Templates

The first inter-modal registrations (source: control scans & target: age-matched T1 paediatric standard space) led to only 8/19 (42%, 6-9 y) and 22/93 (24%, 10-20 y) optimally aligned PET scans which were used to compute Average1. This initial paediatric PET template increased the accuracy of the subsequent registrations, so that the second intra-modality registrations (source: control scans & target: Average1) resulted in an increased number of perfectly aligned scans used to create Average2: 14/19 (74%) and 41/93 (44%).

Comparison of Scenium and SPM8

The results of Scenium/SPM8 pipelines were compared with the MDT diagnosis available for each patient (Supplemental Table 2 for patient diagnosis and results of voxel-wise analyses). **Table 1** reports the results of the Kappa test for both Scenium and SPM8. Overall, Scenium showed substantial agreement with the MDT diagnosis in terms of lateralisation and only moderate agreement for localisation. Conversely, SPM8 achieved an overall substantial agreement in both lateralisation and localisation. An almost perfect agreement was found by SPM8 for localisation in the younger group (0.826) whereas Scenium showed the lowest agreement in the moderate range (0.489).

Fig. 3 reports the comparison of the voxel-wise statistical maps obtained for two representative subjects. In both cases, SPM8 correctly detected the presumed epileptogenic areas located in the right frontal lobe and right temporal lobe, respectively, as reported by the MDT diagnosis. These regions were also highlighted in the Z-score maps from Scenium. However, despite being visible on the maps they did not reach the significance threshold of

<-2 SDs in the ROI-based statistical tables, considered for clinical reporting. Indeed, for subject E22, the most hypo-metabolic region was found in the left temporal lobe with -3 SDs, while the right frontal lobe only had -0.3 SDs. In the case of subject E5, the most hypo-metabolic region was placed in the left parietal region with -2.3 SDs, while the right temporal lobe resulted in -1.0 SDs.

SPM8 Pipeline: Validation with Post-Surgical Seizure-Free Cases

In order to further validate the ad-hoc pipeline based on SPM8, we selected a subgroup of patients who underwent surgical resection of the presumed focus with positive outcome (Engel class I, **Fig. 1**). Lateralisation and localisation of the most significant cluster to the resected area was assessed using post-operative MRI scans or surgery reports (when post-surgical scans were not available). For lateralisation (localisation), SPM8 showed a sensitivity of 67% (67%) for the younger patient group (n=3) and 80% (70%) for the older patient group (n=10). The SPM8-based statistical maps overlaid on the post-operative MRI scans with the resection cavity clearly visible are shown in **Fig. 4** for four representative patients. The area reported as most significant correctly co-localised with the resected area in all cases. For subject E7, the small hypo-metabolic area at the edge of the temporal lobe was shifted to the border of the brain during the registration steps to bring the map back to native space.

To further quantify the degree of overlap, the percentage of voxels falling in the resection cavity was computed. This analysis was carried out on 5/10 subjects with post-surgery MRI scans as one subject had thermal ablation, hence the resection area was not present, while in the other 4 seizure-free patients the statistical cluster did not overlap with the resected area. The percentage of voxels falling in the resection cavity was more than 50% in the majority of cases (**Table 2**). For subject E7, the lower percentage was due to suboptimal registration which caused the statistical map to be shifted to the edge of the brain (**Fig. 4**). Hence, fewer voxels fell into the resection

cavity. For subject E21, the cluster containing the maximum as represented on the SPM8 map only partially covered the lesion (**Fig. 4**), leading to a lower overall percentage within the resected area (34%).

SPM8 Pipeline: Non Seizure-Free Cases

Five subjects were not seizure-free post-surgery (**Fig. 1**). In three of these cases, SPM8-based statistical maps reported a more diffuse hypo-metabolism which extended further than the resected area. In the remaining two cases, the cluster containing the maximum co-localised with the area resected. **Fig. 5** shows the results of the SPM8 analysis for three non seizure-free patients. For patients E10 and E29, SPM8 reported a more extensive hypo-metabolism than the area resected, which might relate to non seizure-free outcome. Patient E29 is of particular note, given the presence of right ventricle dilatation, highlighting a more profound pathology which is likely not to be resolved by the focus resection. Patient E28 represents a case where the statistical map correctly co-localised to the resected area, but the patient is not seizure-free post-surgery.

DISCUSSION

The aim of this work was to provide a reliable observer-independent pipeline for the analysis of paediatric FDG-PET scans, as part of pre-surgical planning in epilepsy. Two age-specific FDG-PET templates in standard paediatric space (as opposed to adult MNI space) were created, representing children between 6-9 and 10-20 years old. Voxel-wise statistics were carried out using the commercial software Scenium (utilising adult normative dataset in MNI space) and a SPM8 pipeline (utilising paediatric templates and datasets). Our results report improved agreement with the MDT diagnosis for both age ranges using the customised SPM8 pipeline with a sensitivity of ~70% for the localisation of hypo-metabolic areas on paediatric FDG-PET scans. Overall, we were able to show that it is essential to use age-matched FDG-PET templates and databases to achieve reliable and accurate results.

Computer assisted reporting is on the rise in several fields of medicine such as breast cancer detection *(14)*, lung cancer screening *(15)* and coronary artery disease identification *(16)* where the use of computer assisted systems together with visual assessment has shown reduction of diagnostic error and false negative rates *(15,16)*. The adoption of these computer systems has shown potential not only to shift from double to single image readings *(14)*, but also in emergency room settings, where automatic systems can alert possible critical condition and flag immediate intervention *(16)*. In the field of neurology, several commercial software applications have been made available by vendors to aid visual reporting of brain FDG-PET scans as part of pre-surgical planning *(12)*. Additionally, previous studies adopted the open source software SPM for automatic voxel-wise analysis of FDG-PET data and inform pre-surgical planning *(2,17,18)*. In most of these analyses, adult standard space and non age-matched control groups were used *(12,17,18)* mainly due to ethical constraints which prevent the acquisition of a normative paediatric PET dataset.

Only two studies reported the creation of an in-house paediatric FDG-PET template obtained using a pseudo-control group of epilepsy patients with normal FDG-PET scans *(2,7)*. However, the actual procedure carried out to build these templates is not adequately described, for the purposes of reproducibility of these analyses. In this work, we outline a detailed two-step registration procedure to create two paediatric templates using a dataset of children without central nervous system diseases. Our results justified the need of a second registration step which was essential to improve the alignment of the control scans to the paediatric standard space, especially for the younger group. In this way, more scans could be included to derive the final template. Our paediatric normative dataset is significantly larger than the ones used in previous studies (n=112 as compared to n=24 *(2)* and n=21 *(7)*) which allowed the creation of templates representing two age groups: 6-9 y and 10-20 y. This age stratification is more accurate than having a unique template representing a wider age range, as it is known that the metabolism and brain size change considerably between 6 and 20 years old *(2)*. Ideally, even smaller age range groups could have been considered (and below 6 y), which was not possible due to low number of younger controls, which were grouped together to guarantee the creation of a reliable template and enough power for the subsequent voxel-wise statistics. In the future, the normal database could be extended by including FDG-PET images from different scanners to mitigate biases introduced by specific acquisition and reconstructions and make the database more widely applicable.

The agreement of the SPM8 pipeline's results with the MDT diagnosis was compared to Scenium, a commercial software package currently used to aid FDG-PET reporting in the clinic. Previous studies compared the voxel-wise results with the visual assessment of FDG-PET data *(2,7,17)*. In this study, Scenium was used as benchmark, to assess its performance and to investigate whether the presented SPM8 pipeline and age-specific templates improve visual

assessment of paediatric FDG-PET data in the clinic. Increased agreement with the MDT diagnosis was found using SPM8 with paediatric templates, thereby supporting the potential of this pipeline as a tool for paediatric FDG-PET reporting. Sensitivity values are in the range of those reported previously, for seizure-free patients *(2,17,18)*. For three non seizure-free cases, we reported a more diffuse hypo-metabolism than the resected area. Hence, we speculate that a more extensive resection, if supported by other assessments and imaging modalities, might have provided a better outcome. With this work, we aim to outline a reliable and robust method which can be applied to a larger post-surgery patient group to compute metrics to investigate the usefulness of this technique (i.e. positive and negative predictive value) and to assess the difference in outcome between resecting more or less than 50% of the significantly hypo-metabolic area *(19,20)*.

There are limitations to using semi-automated reporting methods. Voxel-wise analyses, despite avoiding obvious user dependencies, can introduce new biases due to differences between the cohort of interest and the normal database. This limitation can be mitigated by accurately assessing each registration step in the pipeline, but it cannot be completely avoided, as spatial normalization to a common space is fundamental for subsequent statistical analysis. Another limitation of this study regards the use of SPM8 which is not FDA approved, as opposed to Scenium. However, the latter, as true for commercial software, provides limited flexibility in both the analysis and sharing of the database (a licence is needed). This hampered the complete matching of the steps between the two pipelines. The data were smoothed with a 6-mm and 12-mm kernel in SPM8 and Scenium, respectively. However, we could not modify the smoothing kernel inbuilt in Scenium and we decided to use a different smoothing size in SPM8 to follow the recommended kernel size in literature (e.g. twice/three times the voxel size). Additionally, larger smoothing kernels, like the fixed 12-mm kernel used in Scenium, increase spatial artefacts and can

decrease the sensitivity in detecting epileptogenic areas *(17)*. The cerebellum grey matter uptake was used to carry out intensity normalization in SPM8, because the glucose uptake of this region is usually minimally affected in epilepsy *(3)*. Hence, its mean value was taken for intra-participant intensity normalization rather than using the mean brain uptake (used by Scenium), as this can lead to biases in the detection of hypo-metabolic regions especially if the subject has a global low baseline metabolism.

CONCLUSIONS

In conclusion, we have shown that using data and applications readily available it is possible to provide a more accurate user-independent semi-quantitative method of assessing FDG-PET scans of patients under 18 y, by creating two age-specific templates and using appropriate paediatric control databases. This analysis can be useful to complement the current visual assessment of FDG-PET images carried out in the clinic.

ACKNOWLEDGMENTS This work is supported by the EPSRC-funded UCL Centre for Doctoral Training in Medical Imaging (EP/L016478/1), the Department of Health's NIHR-funded Biomedical Research Centre at UCLH and GOSH, by the MRC and by the ALSAC.

REFERENCES

1. Çataltepe O, Jallo GI. *Pediatric Epilepsy Surgery*. New York, Thieme; 2010;1-6.

2. Archambaud F, Bouilleret V, Hertz-pannier L, et al. Optimizing statistical parametric mapping analysis of 18F-FDG PET in children. *EJNMMI Res*. 2013;3:1–10.

3. Boscolo Galazzo I, Mattoli MV, Pizzini FB, et al. Cerebral metabolism and perfusion in MR-negative individuals with refractory focal epilepsy assessed by simultaneous acquisition of 18F-FDG PET and arterial spin labeling. *NeuroImage Clin*. 2016;11:648–657.

4. Kim YK, Lee DS, Lee SK, Chung CK, Chung J-K, Lee MC. 18F-FDG PET in localization of frontal lobe epilepsy: comparison of visual and SPM analysis. *J Nucl Med.* 2002;43:1167–74.

5. Kim YK, Lee DS, Lee SK, et al. Differential features of metabolic abnormalities between medial and lateral temporal lobe epilepsy: quantitative analysis of (18)F-FDG PET using SPM. *J Nucl Med*. 2003;44:1006–12.

6. Mayoral M, Marti-Fuster B, Carreno M, et al. Seizure-onset zone localization by statistical parametric mapping in visually normal 18F-FDG PET studies. *Epilepsia*. 2016;57:1236–44.

7. Mazzuca M, Jambaque I, Hertz-Pannier L, et al. F-18-FDG PET reveals frontotemporal dysfunction in children with fever-induced refractory epileptic encephalopathy. *J Nucl Med*. 2011;52:40–47.

8. Evans AC, Collins DL, Mills SR, Brown ED, Kelly RL, Peters TM. 3D statistical neuroanatomical models from 305 MRI volumes. *Proc IEEE-Nuclear Sci Symp Med Imaging Conf.* 1993;1813–7.

9. Fonov V, Evans AC, Botteron K, Almli CR, McKinstry RC, Collins DL. Unbiased average age-appropriate atlases for pediatric studies. *NeuroImage*. 2011;54:313–27.

10. Hua C, Merchant TE, Li X, Li Y, Shulkin BL. Establishing age-associated normative

ranges of the cerebral 18 F-FDG uptake ratio in children. *J Nucl Med*. 2015;56:575–9.

11. Jenkinson M, Smith S. A global optimisation method for robust affine registration of brain images. *Med Image Anal*. 2001;5:143–56.

12. Schenk VUB: Scenium v.1 and PET, white paper paper published by Siemens, *Medical Solutions USA, Inc* in 2006;0–11.

13. Viera AJ, Garrett JM. Understanding interobserver agreement: the Kappa statistic. *Fam Med*. 2005;37:360–3.

14. Gilbert FJ, Astley SM, Gillan MGC, et al. Single reading with computer-aided detection for screening mammography. *N Engl J Med*. 2008;359:1675–84.

15. Al Mohammad B, Brennan PC, Mello-Thoms C. A review of lung cancer screening and the role of computer-aided detection. *Clin Radiol*. 2017;72:433–42.

16. Goldenberg R, Eilot D, Begelman G, Walach E, Ben-Ishai E, Peled N. Computer-aided simple triage (CAST) for coronary CT angiography (CCTA). *Int J Comput Assist Radiol Surg*. 2012;7:819–27.

17. Kumar A, Juhasz C, Asano E, Sood S, Muzik O, Chugani HT. Objective detection of epileptic foci by FDG PET in children undergoing epilepsy surgery. *J Nucl Med*. 2010;51:1901–1907.

18. Lee JJ, Kang WJ, Lee DS, et al. Diagnostic performance of 18F-FDG PET and ictal 99mTc-HMPAO SPET in pediatric temporal lobe epilepsy: quantitative analysis by statistical parametric mapping, statistical probabilistic anatomical map, and subtraction ictal SPET. *Seizure*. 2005;14:213–20.

19. Stanišić M, Coello C, Ivanović J, et al. Seizure outcomes in relation to the extent of resection of the perifocal fluorodeoxyglucose and flumazenil PET abnormalities in anteromedial

temporal lobectomy. *Acta Neurochir (Wien)*. 2015;157:1905–16.

20. Vinton AB, Carne R, Hicks RJ, et al. The extent of resection of FDG-PET hypometabolism relates to outcome of temporal lobectomy. *Brain*. 2007;130:548–60.

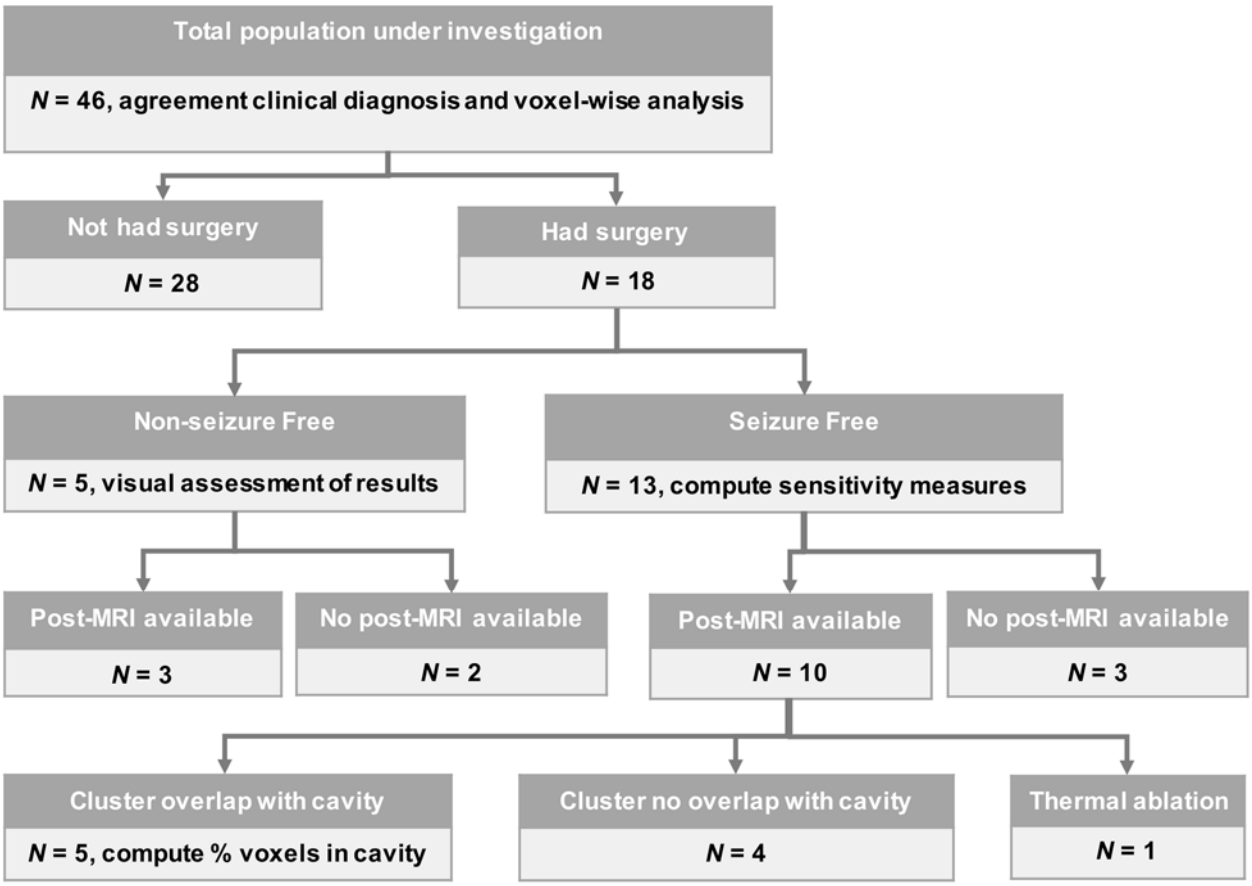

Fig. 1. Population under investigation and corresponding analyses for validating the SPM8 pipeline

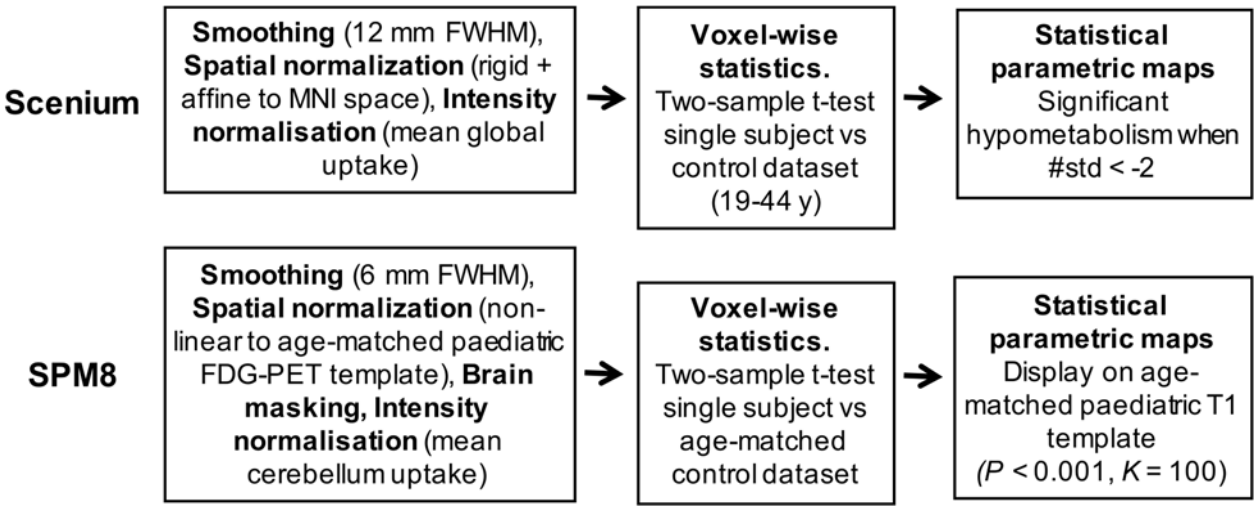

Fig. 2. Pre-processing and statistical analysis steps using Scenium and SPM8

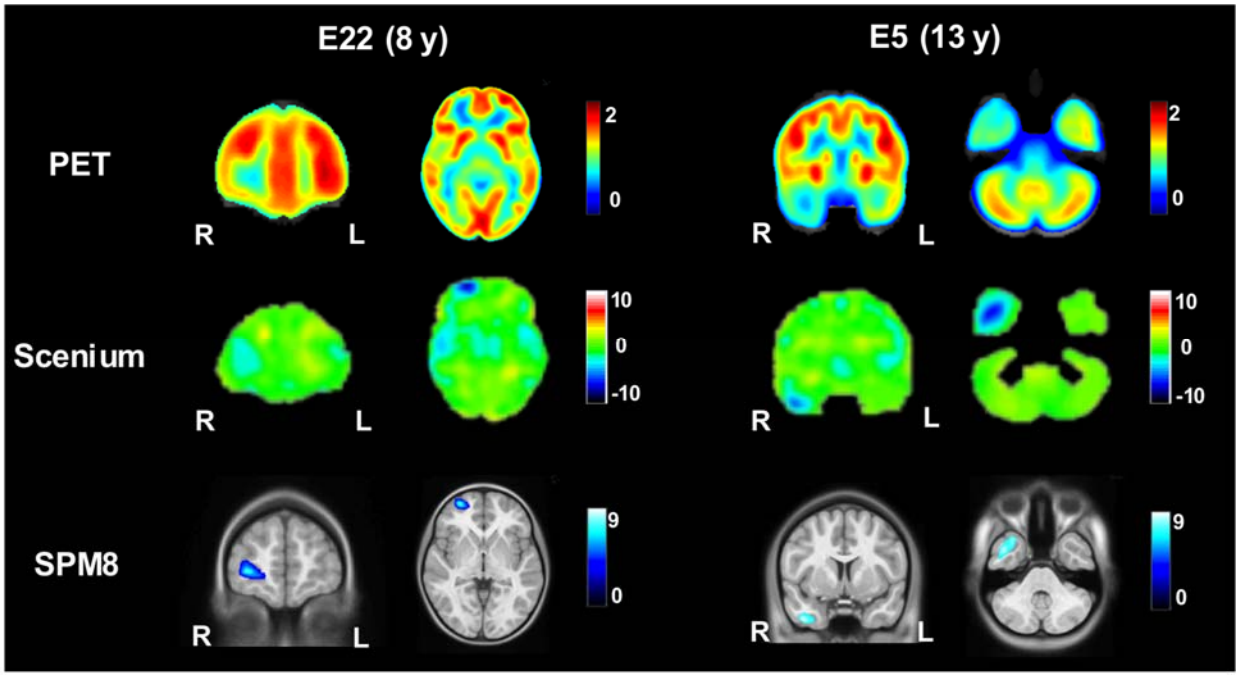

Fig. 3. Comparison of voxel-wise statistical maps of Scenium (Z-score) and SPM8 (T-value). Two representative slices approximately at the same anatomical level were chosen, considering the different size of the standard spaces within Scenium and SPM8

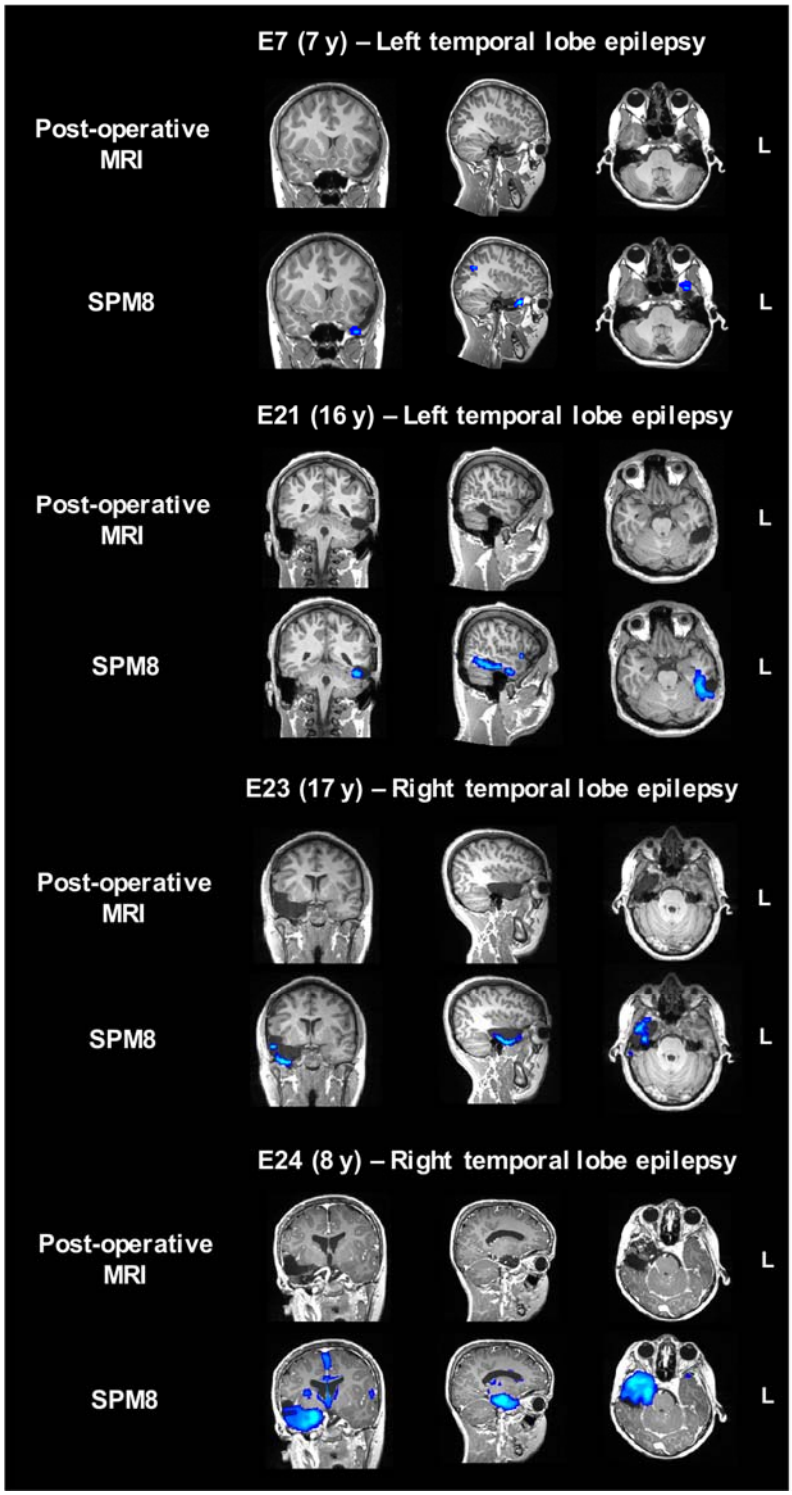

Fig. 4. Pre-surgical SPM8-based statistical maps overlaid on the co-registered post-surgical MRI scans for four representative seizure-free patients

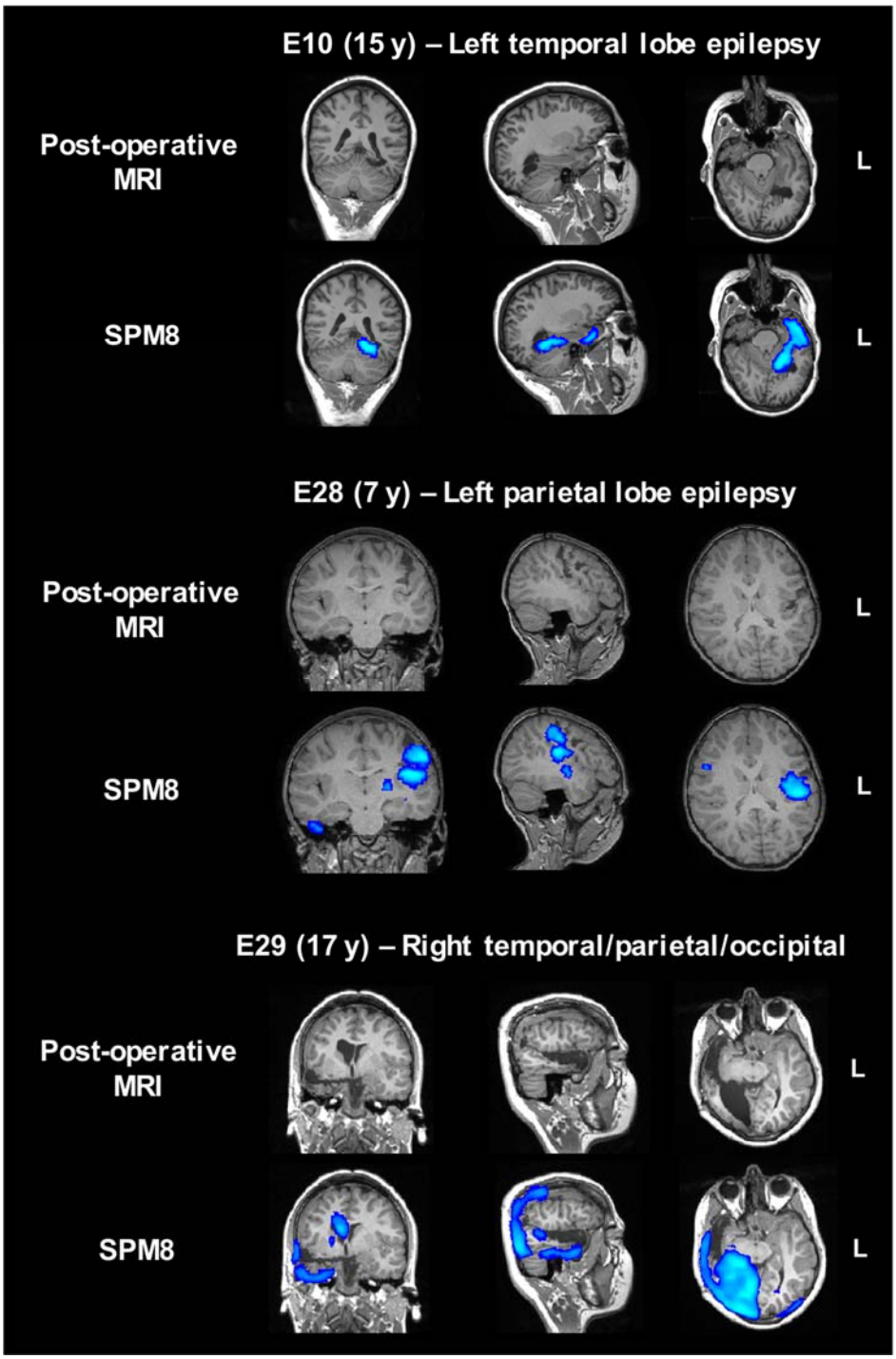

Fig. 5. Pre-surgical SPM8-based statistical maps overlaid on the co-registered post-surgical MRI scans for three representative non seizure-free patients

Table 1. Kappa test results quantifying the level of agreement (lateralising and localising) between each pipeline and the MDT diagnosis for each patient (all subjects n=46, 6-9 y n=16 and 10-17 y n=30)

	Lateralisation		**Localisation**	
	$k_{Scenium}$	**k_{SPM}**	**$k_{Scenium}$**	**k_{SPM}**
All	0.680	0.770	0.536	0.734
6-9y	0.630	0.805	0.489	0.826
10-17y	0.705	0.752	0.555	0.684

Table 2. Proportion of voxels falling in the resection cavity

Subj.	% of voxels falling in the resection cavity
E7	5%
E16	68%
E21	34%
E23	71%
E24	53%

Table 1: Demographic and clinical information of the patient population analysed in this work. The histological information is reported only when available after surgical resection.

Subject	Sex	Age at PET (years)	Location Defined by Multidisciplinary Meeting	MRI lesion	Histology
E1	M	14	Right frontal (cingulate)	Subtle cortical dysplasia in right cingulate gyrus	Presumed dysplasia type 2. Small sample making diagnosis complex
E2	M	10	Reported as normal	Left hemisphere is smaller (particularly temporal lobe)	
E3	M	8	Right frontal	Venous abnormalities. No focal cortical dysplasia	
E4	M	9	Right frontal and left temporal	Negative	
E5	F	13	Right anterior temporal	Slightly reduced brain volume, negative otherwise	Reactive changes and evidence of acquired cortical and white matter damage. No evidence of an underlying lesion to explain epilepsy
E6	M	8	Right temporal	Negative	
E7	M	7	Left temporal	Left mesial temporal sclerosis	Hippocampal sclerosis, granular cellular dispersion
E8	F	15	Right anterior temporal	Negative	The tissue shows reactive changes many of which are related of the placement of intracranial electrodes. No diagnostic features.
E9	F	16	Left frontal	Negative	
E10	F	15	Left temporal	Lesion in left mesial temporal lobe (extend to left hippocampus and parahippocampal gyrus)	Parahippocampal gyrus: low grade glioneuronal tumour favouring a ganglioglioma (WHO grade I)
E11	F	17	Multifocal (bilateral temporal)	Some poverty of grey-white matter differentiation in the right temporal lobe (uncertain significance)	

E12	F	16	Right frontal	Blurring of the cortical and white matter junction involving the left occipitaltemporal gyrus and the inferior parietal lobule, for cortical dysplasia. No other abnormalities (2009 and negative on later scans)	Reactive changes and some acquired damage (invasive monitoring). No diagnostic evidence of a malformation or underlying pathology
E13	F	17	Left anterior temporal	Suspicious area of possible abnormal sulcation with prominent cortical vein in the left parietal lobe (possible dysplasia)	Non-specific features that are frequent in patients with seizures (white matter vascular changes and Chasiln's changes). No specific diagnostic features
E14	F	6	Multifocal	Loss of brain volume (pronounced in cerebellum) Negative	
E15	M	11	Reported as normal	Negative	
E16	F	11	Left anterior temporal	Prominence in the right choroid fissure, no specific features of mesial temporal sclerosis. No lateralising or localising features	Temporal lobectomy, hippocampal sclerosis (ILAE type 1) and granular cell dispersion
E17	F	9	Left frontal	Left cerebral volume loss. Left hemisphere posterior frontal and perisylvian volume loss (Rasmussen's encephalitis)	
E18	M	12	Left frontal	Focal cortical dysplasia (IIB) left middle frontal gyrus	Focal cortical dysplasia type 2b
E19	M	6	Right parietal	Left frontal lobe possible focal cortical lesion, small foci of deep white matter signal change in the peritrigonal regions (mature gliotic scars)	No characteristics of focal cortical dysplasia, small scar. Further examination requested
E20	F	9	Right parietal (patchy)	Asymmetry of grey matter differentiation and white matter signal, poorer in the right frontal lobe. No convincing evidence of focal cortical dysplasia	
E21	M	16	Left posterior temporal	Malformation of cortical development focal cortical dysplasia left temporal sulcus with features of focal cortical dysplasia 2b (signal abnormality extending to the ventricular margins)	Focal cortical dysplasia type 2b

E22	M	8	Right frontal	Right frontal lobe lesion (middle frontal gyrus). Abnormal signal within the cortex along the superior longitudinal fissure and widening of the sulcus	
E23	F	17	Right anterior temporal	Right mesial temporal sclerosis	Hippocampal sclerosis (ILAE type 1) with granule cell dispersion
E24	F	8	Right temporal	Mature brain injury to the adjacent right temporal lobe and frontal lobe	Cortical and white matter calcification, granule cell dispersion, Hippocampal sclerosis (ILAE type 2)
E25	M	17	Right temporal	Negative	
E26	F	17	Left temporal lobe	Left mesial parietal cortical dysplasia and diffuse left temporal lobe abnormalities (left mesial temporal lobe sclerosis)	Hippocampal sclerosis (ILAE type 1), granular cell dispersion and mossy fibre sprouting
E27	M	10	Left posterior insula and post-central)	Negative	Thermal coagulation
E28	F	7	Left parietal operculum and insula	Abnormal cortical folding in the left parietal operculum, plus blurring of grey-white matter junction which is consistent with cortical dysplasia. More extensive bilateral malformation	Focal cortical dysplasia type 2b
E29	F	16	Right temporal/parietal/occipital	Porencephalic dilatation of the right lateral ventricle with gliosis of the right occipital lobe. The right cerebral hemisphere is smaller than the left	Segmental neural loss and gliosis in the hippocampus
E30	M	17	Left anterior temporal	Left cerebral hemisphere is smaller than the right (particularly temporal lobe). Blurring of the cortical grey and subcortical white matter in the anterior temporal pole of the left with associated hippocampal sclerosis (might be focal cortical dysplasia)	Hippocampal sclerosis (ILAE type 1) with granule cell dispersion and mossy fibre sprouting
E31	F	12	Multifocal	Mild while matter bulk with mild prominence of the lateral ventricles and a thin corpus callosum, in keeping with developmental delays. Small non specific left thalamic scar	
E32	F	10	Left precuneous/parietal	Mature region of damage with cortical and white matter scarring in the left mesial parietal lobe which	

				is non specific but could be old infract. Few smaller foci of signal abnormality in the deep white matter of the right frontal lobe, these are not specific
E33	M	15	Left occipital	Area of blurring of the grey/white matter junction in the left mesio-occipital region (focal cortical dysplasia)
E34	M	6	Multifocal	Negative
E35	F	16	Multifocal	Small lesion in the medial aspect of the left thalamus, which is non-specific
E36	F	9	Right frontoparietal	Blurring of the grey-white matter interfaces involving the right frontal lobe and including the frontal opercular region, most marked in the superior frontal gyrus
E37	M	10	Left post central gyrus around motor cortex	Negative
E38	M	16	Right frontal	Negative
E39	F	17	Patchy right hemisphere	Negative
E40	M	6	Right temporal	Patchy, posterior, in temporal pole myelination not complete on both sides, more on the right. Abnormalities in white matter
E41	M	16	Multifocal (bilateral hypometabolism)	Signal in the right temporal white matter and right hippocampus are slightly brighter than the left side, but this can be seizure related. No cortical malformation, no changes in hippocampi, no abnormal diffusion in brain parenchyma
E42	M	14	Multifocal (bilateral hypometabolism)	Right hemisphere is slightly smaller than the left. Immaturity in myelin maturation in the right hemisphere, with poor grey-white matter differentiation (anterior right temporal lobe and anterior parts of the perisylvian cortex)
E43	F	9	Multifocal (left lateralisation)	Negative

E44	F	9	Left temporal	Negative
E45	F	16	Multifocal (bilateral temporal)	Motor cortices a bit abnormal, subtle right motor cortex strip
E46	F	16	Right hemisphere	Enlarged ventricles and swollen right hemisphere. Non-progressive atrophy of the right frontal lobe and the right operculum

Table 2: Clinical diagnosis of each patient and corresponding area highlighted by Scenium and SPM8 pipelines. The cases of disagreement are reported in red.

Subj.	Location Defined by Multidisciplinary Meeting	Results Scenium	Results SPM8
E1	Right frontal (cingulate)	Right parietal	Posterior right frontal
E2	Reported as normal	Multifocal	Right frontal
E3	Right frontal	Right frontal	Right frontal
E4	Right frontal and left temporal	Bilateral frontal	Right frontal and left temporal
E5	Right anterior temporal	Left central/parietal	Right anterior temporal
E6	Right temporal	Right temporal	Left temporal
E7	Left temporal	Left frontal	Left temporal
E8	Right anterior temporal	Right temporal	Right temporal
E9	Left frontal	Left frontal	Left frontal + others Parietal
E10	Left temporal	Left temporal	Left temporal
E11	Multifocal (bilateral temporal)	Multifocal	Multifocal
E12	Right frontal	Left temporal	Left temporal
E13	Left anterior temporal	Left temporal	Left temporal
E14	Multifocal	Multifocal	Multifocal
E15	Reported as normal	Left temporal	Left temporal posterior
E16	Left anterior temporal	Left temporal	Left temporal
E17	Left frontal	Left frontal	Left frontal
E18	Left frontal	Left frontal	Normal
E19	Right parietal	Left frontal	Left operculum/temporal
E20	Right parietal (patchy bilateral)	Patchy bilateral	Patchy bilateral
E21	Left posterior temporal	Left temporal	Left temporal
E22	Right frontal	Left temporal	Right frontal
E23	Right anterior temporal	Right temporal	Right temporal
E24	Right temporal	Right temporal	Right temporal
E25	Right temporal	Right temporal	Right temporal
E26	Left temporal	Left temporal	Left temporal
E27	Left posterior insula and post-central	Left central/	Left posterior insula and post-central
E28	Left parietal operculum and insula	Left frontal	Left parietal operculum and insula
E29	Right temporal/parietal/occipital	Right occipital parietal	Right occipital temporal (wider)
E30	Left anterior temporal	Left parietal	Left temporal (wider)
E31	Multifocal	Multifocal	Multifocal
E32	Left precuneus/parietal	Left parietal	Left precuneus/parietal
E33	Left occipital	Normal	Left occipital
E34	Multifocal (right hemisphere)	Multifocal	Multifocal (right hemisphere)
E35	Multifocal	Multifocal	Multifocal
E36	Right frontoparietal	Right frontoparietal	Right frontoparietal

E37	Left post central gyrus (motor)	Left frontal	Left post central gyrus
E38	Right frontal	Normal	Left frontal
E39	Patchy right hemisphere	Patchy right	Patchy right hemisphere
E40	Right temporal	Right temporal	Right temporal
E41	Bilateral hypometabolism	Bilateral hypometabolism	Bilateral hypometabolism
E42	Bilateral hypometabolism	Bilateral hypometabolism	Bilateral hypometabolism
E43	Left hemisphere (not clear)	Left hemisphere	Left hemisphere
E44	Left temporal	Normal	Left posterior/parietal
E45	Bilateral temporal	Bilateral temporal	Bilateral temporal
E46	Right hemisphere	Right hemisphere	Right hemisphere

The Journal of NUCLEAR MEDICINE

Age-Specific ^{18}F-FDG Image Processing Pipelines and Analysis Are Essential for Individual Mapping of Seizure Foci in Paediatric Patients with Intractable Epilepsy

Bianca De Blasi, Anna Barnes, Ilaria Boscolo Galazzo, Chia-ho Hua, Barry Shulkin, Matthias Koepp and Martin Tisdall

J Nucl Med.
Published online: April 6, 2018.
Doi: 10.2967/jnumed.117.203950

The Journal of Nuclear Medicine is published monthly.
SNMMI | Society of Nuclear Medicine and Molecular Imaging
1850 Samuel Morse Drive, Reston, VA 20190.
(Print ISSN: 0161-5505, Online ISSN: 2159-662X)

SNMMI SOCIETY OF NUCLEAR MEDICINE AND MOLECULAR IMAGING